Optimal Filtering of AC Output Anemometers

J. C. BARNARD, L. L. WENDELL, AND V. R. MORRIS

Pacific Northwest National Laboratory, Richland, Washington

(Manuscript received 7 July 1997, in final form 19 December 1997)

ABSTRACT

The output of pulsed and AC output anemometers suffer from discretization noise when such anemometers are sampled at fast rates (>1 Hz). This paper describes the construction of an optimal filter designed to reduce this noise. By comparing the filtered output from an AC output cup anemometer with a nearby cup anemometer whose output is free from discretization noise, it is shown that the filter significantly reduces the noise. Wind speed time series obtained from the two anemometers are quite similar. Next, deconvolution is applied to the filtered time series to account for the anemometer response. Spectra from the deconvolved time series and a time series measured by a nearby sonic anemometer are compared, and for high-speed flows the spectra from the two instruments match quite well. The time series are also very similar; however, the cup anemometer generally cannot respond to the quick bursts of speed seen by the sonic anemometer. The filtering and deconvolution methods presented here are most appropriate for the high-speed flows relevant to wind energy studies. These methods make it possible to use inexpensive, rugged cup anemometers to measure a high-speed, turbulent wind field up to a frequency of about 5 Hz.

1. Introduction

The wind energy industry has an obvious interest in measuring the wind. The data emanating from such measurements are clearly indispensable for studies ranging from wind resource assessments to turbine fatigue studies. An important consideration for these studies is the type of anemometer chosen for the field campaign. Wind resource assessments require rugged anemometers that can be deployed in the field and left unattended for many months or longer. These anemometers are sampled at relatively low rates (<1 Hz) from which one can capture the mean speed and its standard deviation. In contrast, turbine fatigue studies often require the detailed characterization of the turbulence in the wind and faster sampling is required. Anemometers that are suitable for a wind resource assessment are generally not suitable for fatigue studies and visa versa.

The low-cost, rugged anemometers favored for wind resource assessments often generate their electrical output in the form of a sinusoidal, alternating current (AC) or a pulse train. For these instruments, the *frequency* of the current (or the time density of pulses) is a measure of the wind speed and the wind speed modulates the frequency. We will term these anemometers AC output anemometers, in contrast to direct current (DC) output anemometers in which the *magnitude* of a DC output voltage is proportional to the wind speed. The conversion of the electrical output of an AC anemometer to a wind speed is performed using a demodulation process designed to measure the frequency of the output signal. One particularly easy way of measuring the frequency is through the mechanism of pulse counting. Given a time interval over which the speed is sampled, pulse counting merely counts the number of zero crossings of the sinusoidal output signal. Each time the signal crosses through zero, a ''count'' is recorded, and the total number of counts in the interval is assumed to be linearly proportional to the wind speed over the sampling interval.

Although pulse counting demodulation is simple, this process introduces some noise into the speed measurement. This noise stems from the discrete nature of pulse counting: the measured speed is registered at discrete values proportional to the number of counts, while the actual speed is continuous. The difference between the measured speed (discrete) and the speed that would be measured with a perfect demodulation scheme (providing a continuous speed) defines the discretization noise. The magnitude of the noise increases as the sampling interval becomes smaller, and for purposes that require fast sampling rates, such as measuring turbulence, AC anemometers cannot be used because, among other things, the discretization noise obliterates the small-scale wind speed fluctuations of the turbulent wind field. Figure 1 illustrates the discrete nature of a wind speed time series measured by an AC output anemometer using pulse-counting demodulation. By taking on only dis-

Corresponding author address: Dr. J. C. Barnard, Pacific Northwest National Lab, MSIN K-9 30, P.O. Box 999, Richland, WA 99352. E-mail: jc_barnard@pnl.gov

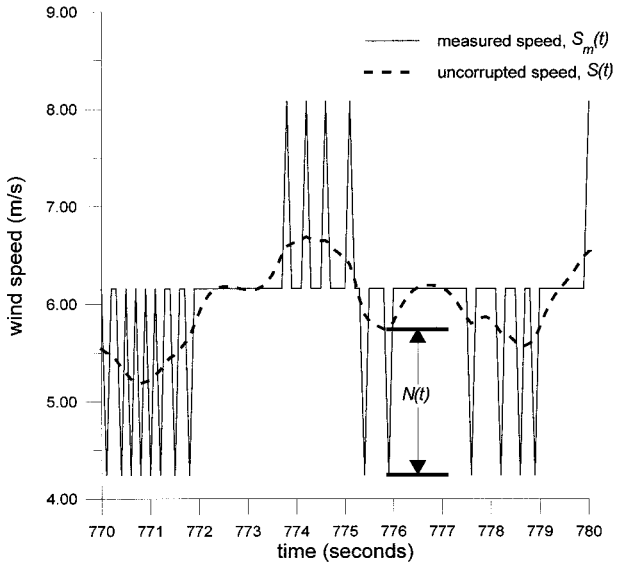

FIG. 1. Wind speed time series from an AC output anemometer sampled at 10 Hz. The discretization noise at $t \approx 776$ is about 1.5 m s^{-1}.

crete values, the speed is distorted and some of the information contained in the wind fluctuations is lost.

The question then becomes, when sampling an AC output anemometer rapidly, can a filter be applied to the data to remove or minimize the discretization noise? If such a filter can be developed, then the use of these anemometers could be extended to the measurement of a portion of the turbulent spectrum (say, with frequencies less than about 5 Hz). The limitations imposed by the anemometer's response (i.e., distance constant) do not allow the measurement of the full spectrum of turbulence. However, for many wind energy applications related to turbine fatigue, such as rotational sampling (Connell 1981; George and Connell 1984), the low-frequency part of the turbulent spectrum with frequencies less than about 5 Hz (roughly the timescale for rotational sampling) is all that is required. Furthermore, it may be possible to restore some of the higher-frequency part of the spectrum by compensating for the anemometer response through deconvolution. This procedure will be briefly discussed at the end of this paper.

We cannot pretend here, however, that the performance of the AC output cup anemometer can ever approach that of a sonic anemometer for measuring the full spectrum of wind turbulence. We are simply seeking an inexpensive, rugged alternative to the sonic anemometer for applications in which only the lower frequencies of the turbulence spectrum are desired. Use of AC output anemometers could therefore allow cost savings in measurement programs designed to measure this part of the turbulence spectrum in two ways: first, the cost of the anemometer would be relatively small, and second, its reliability would permit long-duration field deployment with minimal maintenance costs. These criteria led to the successful deployment of the Maximum cup (16-pole AC output) anemometer in the U.S. Department of Energy's (DOE) Turbulence Characterization Program (Wendell 1998).

2. Discretization noise and optimal filtering

As mentioned above, discretization noise results from a pulse-counting demodulation scheme in which each zero crossing of AC anemometer's output sine wave constitutes a count. The number of counts over the sampling time interval, Δt, is recorded by the datalogger, and the speed for this interval is determined by multiplying the number of counts times a conversion factor, $C/2\Delta t$, where C is a calibration constant. Because of the discrete nature of the pulse-counting operation, it is only possible to measure the wind speed at discrete speed levels, $n \cdot (C/2\Delta t)$, $n = 0, 1, 2, 3, \ldots$, where the levels are separated by the discretization interval $C/2\Delta t$. Each measured speed, $S_m(t_j)$, must be registered at one of these levels. (The time t_j lies in the center of the sampling interval.) If the uncorrupted speed, $S(t)$, is defined as the speed that would be measured if discretization were absent, then we can define a "discretization noise," $N(t)$, as the difference between $S_m(t)$ and $S(t)$, that is, $N(t) = S(t) - S_m(t)$. This noise is pointed out in Fig. 1.

For sampling intervals that are large, the discretization interval $C/2\Delta t$ is very small, and the discretization noise is insignificant. However, as the sampling interval decreases, the discretization interval increases, and for the fast sampling rates needed to measure turbulence, the discretization noise may become unacceptably large. For example, sampling at 10 Hz with a typical value of C (0.3819 m s^{-1} Hz^{-1}) gives a discretization interval of about 1.9 m s^{-1}, and the discretization noise may be as large as this value. Noise of this magnitude will grossly distort the spectrum of turbulence. (Examples of this distortion will be shown later.) If the time series is to be of use for turbulence measurements, it is necessary to somehow rid the series of the discretization noise.

One way of reducing this noise is by convolving the wind speed time series with an optimal filter designed to minimize the discretization noise. The derivation of an optimal (Wiener) filter is described by Press et al. (1992) and in the time domain, the filter $f(t)$ may be found by solving the equation

$$f(\tau) * [\sigma_S^2 \rho_S(\tau) + \sigma_N^2 \rho_N(\tau)] = \sigma_S^2 \rho_S(\tau), \qquad (1)$$

where the asterisk ($*$) denotes a convolution. From this formula one may see that the filter depends on two parameters: the autocorrelation of the uncorrupted speed $\sigma_S^2 \rho_S(\tau)$ and the autocorrelation of the discretization noise $\sigma_N^2 \rho_N(\tau)$. In Eq. (1), the autocorrelations have been expressed as a combination of a variance, σ^2, multiplied by an autocorrelation coefficient, ρ. For the discretization noise, it is easier to find each component of the autocorrelation rather than finding the autocorrelation

directly; see below. (We assume that the wind speed time series under consideration is stationary so that the autocorrelations may be regarded at a function of lag time τ only.)

The crux of the filter construction is the determination of these parameters; once these parameters are known, numerical calculation of the filter may then proceed using Eq. (1). Note that parameters σ_S^2 and $\rho_S(\tau)$ are properties of the uncorrupted speed, yet we do not know this speed—and if we knew this speed in advance, there would be no need for the filter! Fortunately, as we shall demonstrate below, it is still possible to ascertain these parameters without detailed knowledge of the uncorrupted speed.

3. Finding the filter parameters

We start by finding σ_N^2, the variance of the discretization noise. The path that leads to the variance is a multistep process in which the penultimate result is the establishment of the probability distribution for the noise $P_N(N)$. Simple integration then yields σ_N^2. The path begins by assuming that the uncorrupted speed remains approximately constant over the sampling interval. A consideration of the pulse-counting process shows that the measured, discrete speed can take on one of two values. These values are the discrete levels that bracket $S(t)$. (Henceforth, we shall drop the explicit dependence of the variables on time unless required for clarity.) Denote these upper and lower levels as S_n and S_{n-1}, respectively, so that $S_{n-1} \le S \le S_n$ and $S_n - S_{n-1} = \Delta S_m$, where ΔS_m is the discretization interval ($C/2\Delta t$). Thus, for the given speed S, the discretization noise can take on only two values—either a positive error, $N_+ = S - S_{n-1}$, or a negative error, $N_- = S_n - S$. The average of these errors over a very large number of sampling intervals must be zero. For the average to be zero, the fraction of intervals for which the error is N_+ must be $(S - S_n)/\Delta S_m$, and the fraction of intervals for which the error is N_- must be $(S - S_{n-1})/\Delta S_m$. To express this mathematically, we may write the conditional probability of the error given that the uncorrupted speed is S, $P_{N|S}$, as

$$P_{N|S}(N|S) = \begin{cases} \dfrac{S_n - S}{\Delta S_m}\delta[N - (S - S_{n-1})], & N = S - S_{n-1}, \\ \dfrac{S - S_{n-1}}{\Delta S_m}\delta[N - (S - S_n)], & N = S - S_n, \end{cases} \tag{2}$$

where δ is the Dirac delta function. [We have used the Dirac delta function to cast a discrete probability distribution in continuous form. Note that $\int_{-\infty}^{\infty} P_{N|S}(N|S)\,dN = 1$, and that $\int_{-\infty}^{\infty} P_{N|S}(N|S)N\,dN) = 0$, as required.] The probability distribution for the error $P_N(N)$ is given by

$$P_N(N) = \int_0^{\infty} P_{N|S}(N|S)P_S(S)\,dS, \tag{3}$$

where $P_S(S)$ is the probability distribution of the uncorrupted speed. For $P_S(S)$ we assume a standard Gaussian distribution:

$$P_S(S) = \frac{1}{\sqrt{2\pi}\,\sigma_S} e^{-(S-\overline{S})^2/2\sigma_S^2}, \tag{4}$$

where $\overline{S}$ is the mean speed over the time period in question.

Although turbulent phenomena are not strictly Gaussian (Panofsky and Dutton 1984), the deviation from Gaussian is often small, particularly for the large, sustained wind speed regimes relevant to the wind energy industry. Of even greater importance, the exact distribution shape has a negligible bearing on our results if the breadth of the distribution is wider than about half the discretization interval or $\sigma_s \gtrsim \Delta S_m/2$. This criterion easily holds for wind energy applications.

An integration of Eq. (3) using Eqs. (2) and (4) yields

$$P_N(N) = \begin{cases} \left(1 - \dfrac{N}{\Delta S_m}\right) \displaystyle\sum_{n=1}^{\infty} \frac{1}{\sqrt{2\pi}\,\sigma_S} e^{-(S-\overline{S})^2/2\sigma_S^2}, \\ \qquad 0 \le N \le \Delta S_m, \\ \left(1 + \dfrac{N}{\Delta S_m}\right) \displaystyle\sum_{n=1}^{\infty} \frac{1}{\sqrt{2\pi}\,\sigma_S} e^{-(S-\overline{S})^2/2\sigma_S^2}, \\ \qquad -\Delta S_m \le N \le 0. \end{cases} \tag{5}$$

The sum in Eq. (5) represents a numerical integration of the Gaussian distribution with a mesh spacing of ΔS_m, and for ''wide'' distributions that span many mesh points (i.e., $\sigma_S \gtrsim \Delta S_m/2$), the sum is equal to $1/\Delta S_m$ [because the numerical integration over all S, $\Delta S_m \sum_{n=1}^{n=\infty} P_S(S_n)$, is approximately equal to 1]. Here, $P_N(N)$ then assumes the particularly simple form

$$P_N(N) = \begin{cases} \left(1 - \dfrac{N}{\Delta S_m}\right)\dfrac{1}{\Delta S_m}, & 0 \le N \le \Delta S_m, \\ \left(1 + \dfrac{N}{\Delta S_m}\right)\dfrac{1}{\Delta S_m}, & -\Delta S_m \le N \le 0. \end{cases} \tag{6}$$

This is a triangular distribution with a base of $2\Delta S_m$ and a height $1/\Delta S_m$; the distribution is shown in Fig. 2.

One may confirm that the noise distribution is indeed triangular by using actual wind data. Suitable data for this confirmation were collected in 1992 as part of a field test of various anemometers performed by Pacific Northwest National Laboratory (PNNL). We briefly digress and discuss these data here. On a boom perpendicular to the prevailing wind direction, PNNL mounted several anemometers including a Maximum cup anemometer (model 160; abbreviated here as Max160) and

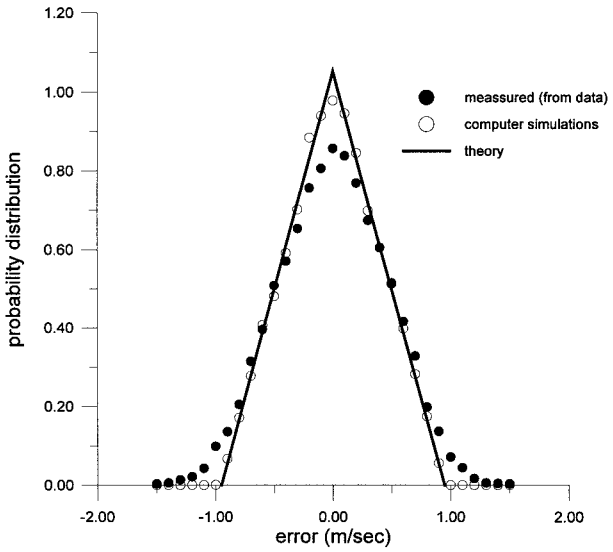

FIG. 2. Triangular probability distribution derived from theory (line), computer simulations (open circles), and data (case 3, solid black dots).

an R.M. Young cup anemometer (model 12012; abbreviated here as RMY.) These anemometers were placed within 2 m of each other. The distance constants are 2.3 and 3 m for the RMY and Max160 anemometers, respectively. (As will be apparent below, the differing distance constants somewhat complicate the comparison of the two instruments.) The output of the RMY anemometer is a DC voltage and the subsequent signal processing of this voltage did not induce discretization noise, while the Max160 is an AC output anemometer and suffers from discretization noise. Both anemometers were sampled at 5 Hz using the same datalogger. Four cases of data will be used in this paper; these cases cover a range in wind speeds and standard deviations. The cases are listed in Table 1.

From these measurements one can infer a ''measured'' discretization noise by subtracting the RMY anemometer's wind speed from the discrete speed registered by the Max160/datalogger combination. This subtraction is performed for each sampling time (0.2 s). Obviously, this procedure can only yield an approximate discretization noise because, among other things, the anemometers sample slightly different winds. The measured error was then binned at intervals of 0.1 m s^{-1} and normalized to form an empirical probability distribution; this distribution is displayed by the black dots in Fig. 2. For the data presented here, we use case 3. (The discretization interval was 0.95 m s^{-1}.) From this figure, it is evident that the empirical probability distribution matches the simple theoretical distribution reasonably well.

To investigate further the shape of the error distribution, computer simulations of the AC anemometer with the pulse-counting demodulation were performed. The simulations began with a simulated wind time series

TABLE 1. Data cases.

Case	Nominal speed (m s^{-1})	RMY σ (m s^{-1})	Max160 σ (m s^{-1})	Duration (min)
1	2	0.91	0.97	15
2	4	0.76	0.85	60
3	8	1.69	1.70	60
4	13	2.15	2.12	60

(Veers 1988) that was convolved with an approximation of the instrument response function to account for the instrument's distance constant. This time series, termed the DC series, represents the speeds measured by a DC output anemometer that is free of discretization noise. Then, to mimic the measurement of the wind by an AC output anemometer, the DC time series was converted to a sinusoidal output and this output was demodulated. We call this time series the AC time series. Both time series account for the instrument response, but the AC series also contains discretization noise. We can therefore calculate the simulated discretization noise by subtracting one series from the other. The resulting noise distribution obtained over a range of speeds is also shown in Fig. 2; the simulations do not include any measurement errors and unequivocally exhibit a triangular distribution. This fact, along with the evidence from the actual measurements presented above, strongly suggest that the discretization noise is modeled reasonably well by a triangular probability distribution.

Once the form of the noise probability distribution is established, σ_N^2 is easily calculated:

$$\sigma_N^2 = \int_{-\infty}^{\infty} P_N(N) N^2 \, dN = \frac{\Delta S_m^2}{6}. \tag{7}$$

For a discretization interval of 0.95 m s^{-1}, σ_N^2 is 0.15 (m s^{-1})^2.

To find the autocorrelation coefficient ρ_N, we relied solely on computer simulations because we could not find any simple analytical path leading to this quantity. The simulations reveal that ρ_N is given by the expression

$$\rho_N(\tau) = \begin{cases} 1, & \tau = 0, \\ -\dfrac{1}{2}, & \tau = \pm\Delta t \\ 0, & \text{otherwise}, \end{cases} \tag{8}$$

where τ is the lag time. (In a manner analogous to the procedure described above, actual wind data were used to show that this expression is an adequate representation of the true autocorrelation coefficient.)

Next, we turn our attention to the parameters associated with the uncorrupted speed. In Eq. (1) the product of σ_S^2 and $\rho_S(\tau)$ appears and we only need to find this product. Because the measured speed is equal to the uncorrupted speed minus the error [i.e., $S_m(t) = S(t) - N(t)$] we may write

$$\begin{aligned}\sigma_m^2\rho_m(\tau) &= \overline{S_m(t)S_m(t+\tau)},\\ &= \overline{S(t)S(t+\tau)} + \overline{N(t)N(t+\tau)}\\ &\quad - (\overline{S(t)N(t+\tau)} + \overline{N(t)S(t+\tau)}),\\ &= \sigma_S^2\rho_S(\tau) + \sigma_N^2\rho_N(\tau)\\ &\quad - (\overline{S(t)N(t+\tau)} + \overline{N(t)S(t+\tau)}), \quad (9)\end{aligned}$$

where the overbar represents a time average, τ is the lag time, $\sigma_m^2\rho_m(\tau)$ is the autocorrelation of the measured speed, and the term $\overline{S(t)N(t+\tau)} + \overline{N(t)S(t+\tau)}$ is a cross correlation between S and N. It was impossible for us to find a analytic expression for the cross correlation, and we again resorted to computer simulations to show that this term is zero for all lags. (For τ equal to zero, the cross correlation simply becomes the covariance between S and N. This quantity can be shown to be zero using analytical methods. Thus, the error and the uncorrupted speed are uncorrelated.) The expression for $\sigma_m^2\rho_m(\tau)$ is then

$$\sigma_m^2\rho_m(\tau) = \sigma_S^2\rho_S(\tau) + \sigma_N^2\rho_N(\tau). \quad (10)$$

Because $\sigma_m^2\rho_m(\tau)$ can be calculated from the measurements and $\sigma_N^2\rho_N(\tau)$ is known from Eqs. (7) and (8) above, we therefore know $\sigma_S^2\rho_S(\tau)$, and all the filter parameters have been discovered. We are now left with the task of calculating the filter shape using Eq. (1).

The calculation of the filter is straightforward and can be done in either Fourier space (see Press et al. 1992) or in the time domain [Eq. (1)]. Whether one solves for the filter in Fourier space or in the time domain is a matter of convenience. Because we hope to implement the filter on a datalogger (on which a fast Fourier transform may be impossible), we choose the time domain and Eq. (1) is solved numerically. By dividing Eq. (1) by σ_N^2 the filter equation takes on the form

$$f(\tau) * [\alpha\,\rho_S(\tau) + \rho_N(\tau)] = \alpha\rho_S(\tau), \quad (11)$$

where α $(=\sigma_S^2/\sigma_N^2)$ serves as a signal-to-noise ratio. Equation (11) forms the basis of a numerical solution scheme for the filter. Assuming that we have a time series composed of $2M + 1$ points, we may then write Eq. (11) in discrete form for the lag times, $\tau = 0, \pm\Delta t, \pm 2\Delta t, \ldots, \pm M\Delta t$; the $2M + 1$ equations are

$$\begin{aligned}&\sum_{k=-M}^{k=M} f(k\Delta t)(\alpha\rho_S[(j-k)\Delta t] + \rho_N[(j-k)\Delta t])\\ &\quad = \alpha\rho_S(j\Delta t), \qquad j = -M, M. \quad (12)\end{aligned}$$

{Equation (12) assumes cyclic redundancy for ρ_S and ρ_N so that, e.g., $\rho_S(k\Delta t) = \rho_S[(k + 2M + 1)\Delta t]$}. Most of these $2M + 1$ equations can be discarded because the filter function is virtually zero for all $|j| > L$ with $L \ll M$. We are then left with the $2L + 1$ equations that may be solved for the $2L + 1$ unknowns $f(j\Delta t)$, $j = 0, \pm 1, \ldots, \pm L$. A further reduction in the computational burden may be obtained by exploiting symmetry so that we only solve for one side of the filter. This results in a reduced system of only $L + 1$ equations; experience has shown that good results may be obtained where L is about equal to 10. The reduced system of equations may be solved quickly by any of the standard methods such as a lower–upper (LU) decomposition. Equation (12) requires an expression for ρ_S. This quantity is determined by first finding the autocorrelation of the measured speed $\sigma_m^2\rho_m(\tau)$ and then using Eqs. (10), (7), and (8) to find the autocorrelation of the uncorrupted speed $\sigma_S^2\rho_S(\tau)$, from which ρ_S follows immediately. Given that only small number of points L are required to solve Eq. (12), it is only necessary to find $\sigma_m^2\rho_m(\tau)$ for lag times from $\tau = 0$ to $\tau = L\Delta t$, and this quantity may be rapidly calculated without resorting to a fast Fourier transform.

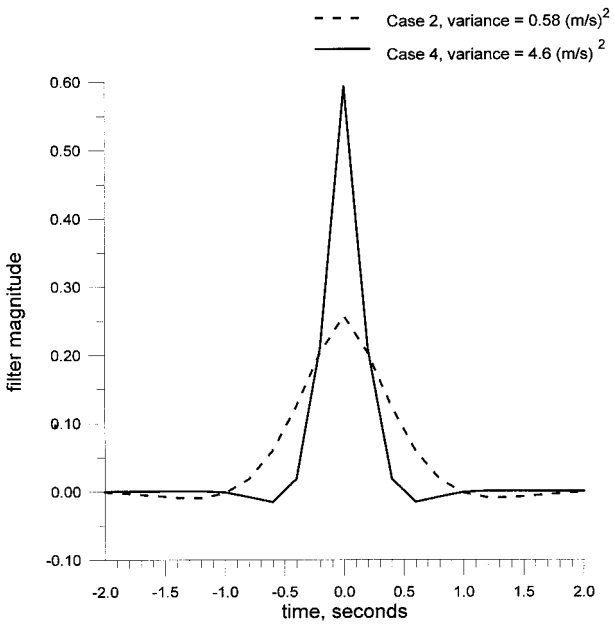

FIG. 3. Optimal filters derived for case 2 [variance = 0.58 (m s^{-1})^2] and case 4 [variance = 4.6 (m s^{-1})^2] listed in Table 1. Note that the filter broadens as the variance decreases.

When we first applied the filter to a corrupted wind time series, we noticed that the spectrum of the final filtered time series had a slight but spurious oscillation at the very highest frequencies. This oscillation was caused by noise that contaminated the filter, which in turn was transmitted to the high-frequency part of the time series when the filter was applied to the series. We found a simple way of eliminating this noise by using a smoothed representation of ρ_S. We fit a line to ρ_S so that ρ_S is represented in Eq. (12) by the simple function $1 - \beta|n\Delta t|$ $(n = -L, \ldots, 0, \ldots, L)$, where β is the slope of the line. Filters calculated using this representation were very ''smooth,'' and the oscillations in the filtered time series spectra were no longer evident.

So we now ask, what does the filter look like? The optimal filters for two of the data cases listed in Table 1, cases 2 and 4, are plotted in Fig. 3. For case 2, the

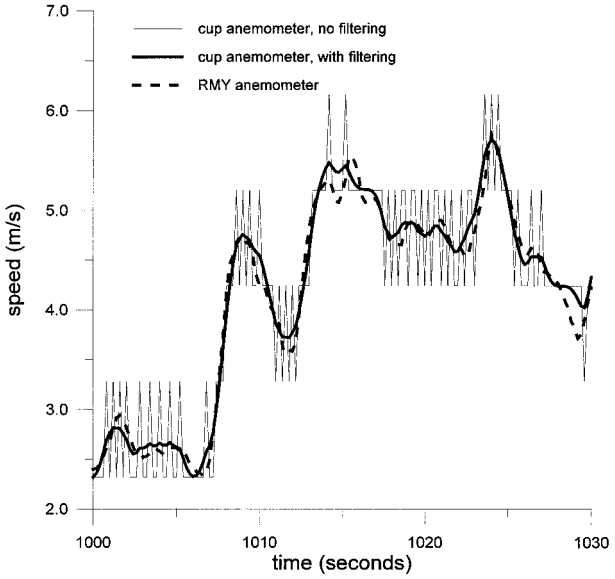

FIG. 4. Unfiltered, filtered, and RMY time series for case 2.

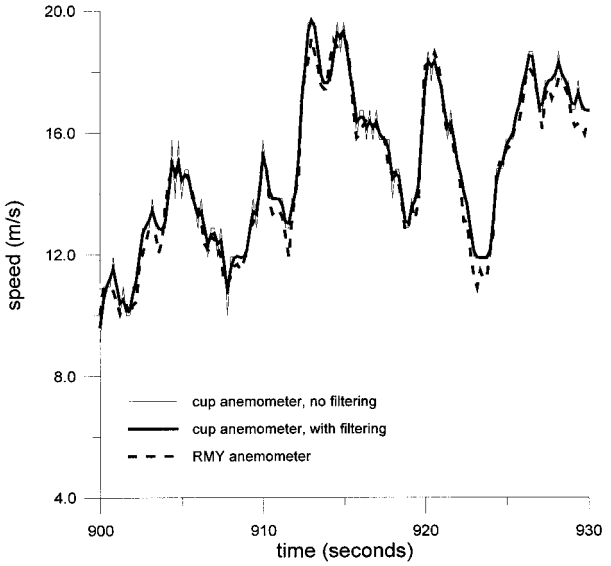

FIG. 5. Unfiltered, filtered, and RMY time series for case 4.

signal-to-noise ratio [as indicated by $(\sigma_m^2 - \sigma_N^2)/\sigma_N^2 = \sigma_S^2/\sigma_N^2 = \alpha$] is relatively low and for case 4 this ratio is much higher. The figure indicates that as the signal-to-noise ratio increases, the filter becomes more narrow. This behavior is expected; for example, in the limiting case $\alpha \to \infty$ (no noise) the filter would become very narrow (a Dirac δ function). Note that the filters are symmetric about zero and therefore they will alter the magnitude but not the phase of the unfiltered wind speeds. Of course, the critical test of the filter performance comes from a comparison of filtered data—an approximation of the uncorrupted speed—to an independent measurement of the uncorrupted speed. We describe this comparison below.

4. Filter performance

Table 1 lists the four cases used to evaluate the filter performance. We show a portion of the unfiltered, filtered, and RMY anemometer time series in Figs. 4 and 5 for case 2 (4 m s^{-1} nominal speed) and case 4 (13 m s^{-1} nominal speed), respectively. As mentioned previously, the RMY anemometer acts as a standard of comparison with which to compare the filtered time series. For the sake of brevity, we call this the ''true'' speed.

Of these two figures, perhaps Fig. 4 is the most interesting. In this figure the discrete pattern of the unfiltered speed is unmistakable, and it is of the same magnitude as the standard deviation of the wind speed. The filter can extract from this pattern a filtered speed that tracks the true speed quite well. (This close tracking is exhibited throughout the entire time series.) In this case we could conclude on a qualitative basis that the filter performance is good.

The wind speed time series in Fig. 5 are from a higher wind regime with a much greater variance. For large variances the effect of the speed discretization is not as noticeable. In fact, one could say that the discretized speed matches the true speed with some fidelity. However, the filtered speed tracks the true speed somewhat better, which again demonstrates the improvement obtained by the use of the filter.

Spectra of the unfiltered, filtered, and true speeds are shown for case 2 (nominal speed 4 m s^{-1}) and case 4 (nominal speed 13 m s^{-1}) in Figs. 6 and 7, respectively. For both cases, the spectra of all three time series track each other quite closely until the discretization noise begins to manifest itself in the unfiltered spectrum. This

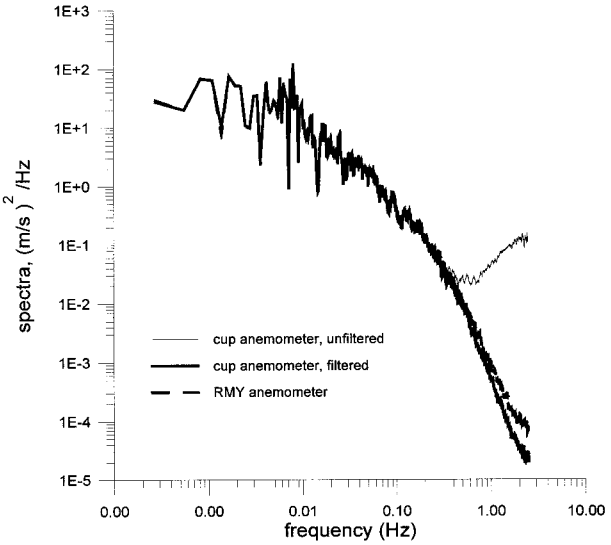

FIG. 6. Spectra of the unfiltered, filtered, and RMY time series for case 2.

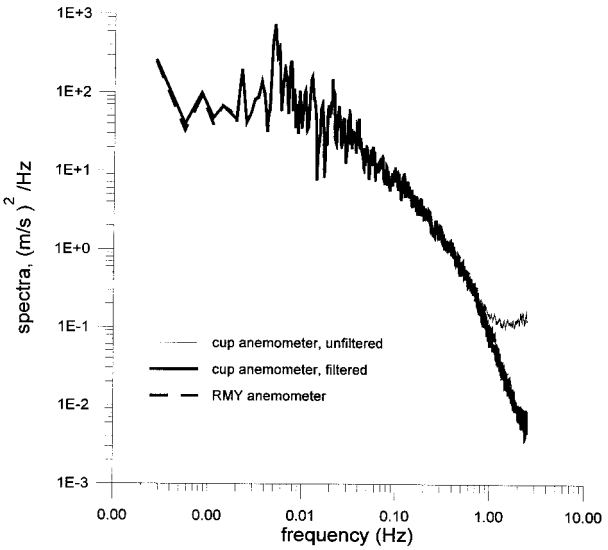

FIG. 7. Spectra of the unfiltered, filtered, and RMY time series for case 4.

occurs at about a frequency of somewhat less than 1 Hz for both the low- and high-speed cases. At this frequency the unfiltered spectrum turns up and increases in magnitude due to the discretization noise. For both cases illustrated here, the filter does an excellent job of reducing the effects of the discretization noise while apparently not materially affecting other parts of the spectrum. The filtered and unfiltered spectra match each other reasonably well over the entire range of the spectrum for case 4 (at least when viewed on a log–log plot), while for case 2 a slight discrepancy between the spectra occurs for frequencies larger than about 0.5 Hz.

The fact that the magnitude of the spectra of the filtered cup is a little less than that of the RMY anemometer is reflected in the variances of the filtered and RMY times series; these are shown in Table 2. In all cases the variances derived from the filtered time series are lower than the corresponding variances obtained from the RMY anemometer. This discrepancy is caused in part by the filter that acts mostly on the less energetic, high-frequency part of the time series but still reduces the variance. Another contributing factor leading to an apparent reduction in variance is the difference in response characteristics between the Max160 and RMY anemometers. The larger distance constant of the Max160 (3 versus 2.3 m for the RMY instrument) would cause the Max160 spectrum to decrease faster than the RMY spectra as the frequency increases. (This roll-off would be observed in case 4 if the spectra were extended to higher frequencies.) One way of removing the effect of the instrument response is through the process of deconvolution, which is discussed below.

5. Deconvolution

Collins and Hunter (1992) describe a way of removing the instrument response from a wind speed time

TABLE 2. Variances of the unfiltered, filtered, and RMY time series.

Case	Nominal speed (m s^{-1})	Max160 σ^2 unfiltered (m s^{-1})^2	Max160 σ^2 filtered (m s^{-1})^2	RMY σ^2 (m s^{-1})^2
1	2	0.95	0.79	0.82
2	4	0.72	0.56	0.58
3	8	2.89	2.72	2.86
4	13	4.51	4.32	4.63

series using a particularly simple deconvolution method. [For this paper, we employ their method II that assumes that the anemometer is a first-order linear system, i.e., see Eq. (12) in Kristensen and Lenschow 1988.] Briefly, the filtered wind speed time series, denoted here by S, is acted upon by the two-point deconvolution filter,

$$U_n = c_1 S_{n-1} + c_2 S_n, \tag{13}$$

to produce a deconvolved time series, U_n. In this expression S_{n-1} and S_n are the filtered speeds at time steps $(n - 1)\Delta t$ and $n\Delta t$, respectively, and U_n is the deconvolved speed. The coefficients c_1 and c_2 are given by

$$c_1 = -\frac{e^{-U_{n-1}\Delta t/D}}{1 - e^{-U_{n-1}\Delta t/D}} \quad \text{and} \quad c_2 = \frac{1}{1 - e^{-U_{n-1}\Delta t/D}}, \tag{14}$$

where D is the anemometer's distance constant and U_{n-1} is the deconvolved speed at the time step $(n - 1)\Delta t$. We found that this simple filter worked reasonably well for recovering the high-frequency part of the wind speed spectrum for high-speed, high-variance flows. For low speeds (<5 m s^{-1}), the filter tended to overcorrect, occasionally producing large and unphysical swings in the deconvolved wind speed. To avoid this problem, we shut off the deconvolution whenever the speed dropped below 5 m s^{-1}. (For this paper, this procedure is justified because the wind energy community is not generally interested in such low wind speeds.)

To evaluate the combination of cup filtering and subsequent deconvolution, the filtered and deconvolved wind speeds must be compared with an anemometer that possesses a very fast response time so that the entire turbulent spectrum can be captured (henceforth we shall call the filtering and deconvolution process FD). Such an opportunity was afforded us during an informal anemometer evaluation that was performed under the auspices of the DOE's Turbulence Characterization Program. For this evaluation, an Applied Technologies, Inc. sonic anemometer and the Max160 cup were mounted at the 20-m level at a tower located in the Tehachapi Pass area of California. The two instruments were separated horizontally by about 1.4 m. Samples of wind data from 37 half-hour periods are available. The wind speeds varied from about 6 to 18 m s^{-1}, and the standard deviations varied over a range of about 0.5–5 m s^{-1}; this is a very turbulent site. The anemometers were both

TABLE 3. Data cases—Tehachapi Pass.

Case	Nominal speed (m s^{-1})	Sonic σ (m s^{-1})	Max160 σ unfiltered (m s^{-1})	Duration (min)
1	9	0.96	1.2	30
2	16	4.9	4.5	30

sampled at 10 Hz. Such a high sampling rate subjects the FD method described here to a very harsh test.

For the sake of brevity, we will not show the results from all 37 cases but just illustrate typical results using the two cases listed in Table 3. These cases represent a low-speed, low-variance case and a high-speed, high-variance case. These two cases bracket the performance of the FD routines. For all 37 cases the average sonic speed and the average cup speed were very close and there was no evidence of gross cup overspeeding. However, the average cup speed was generally slightly higher than the sonic speed. For example, in case 2 of Table 3 the average sonic and cup speeds were 15.72 and 16.00 m s^{-1}, respectively. The small increase of the cup speed over that of the sonic, about 1.8%, could be due to calibration differences between the two instruments or a small amount of overspeeding. (The issue of cup overspeeding is examined in the appendix.)

The important issues regarding the performance of the FD process are whether the variance of the true wind speed, as measured by the sonic anemometer, can be fully recovered and whether the spectrum of the recovered wind speed is correct. For our two illustrative examples the first issue is addressed in Table 4. In this table the variance of the sonic anemometer (assumed to be the ''true'' variance) is listed as well as the variances of the cup anemometer as it passes through the stages of filtering and deconvolution. We first note that for both cases the variance that is obtained after filtering but before deconvolution is much less than sonic variance. It then falls to the deconvolution to recover this lost variance.

We see, unfortunately, that the deconvolution is only able to recover a small fraction of the ''lost'' variance. This feature of the deconvolution is illustrated in Fig. 8 in which for all 37 cases the sonic variance is plotted versus the cup variance with deconvolution (open circles) and without deconvolution (crosses). In all cases the cup variance is lower than the sonic variance. We tried to determine empirically why this occurred and to this end, we examined the spectra $P(f)$, plotted as $fP(f)$ versus $\log(f)$ (so that the variance is the area under the spectrum). From this examination, we concluded that although the shape of the cup and sonic spectra were about the same, the amplitude of the cup spectra was a little too small (as expected), and this small discrepancy was roughly constant with frequency, particularly for the high-speed cases. (Why the cup cannot fully keep up with the sonic at the low frequencies is something we cannot yet explain.) If a cup's spectrum was multiplied by a constant, then the match between the sonic and cup spectra was much improved. This suggested the following *empirical* (and simple) correction to the cup's speed:

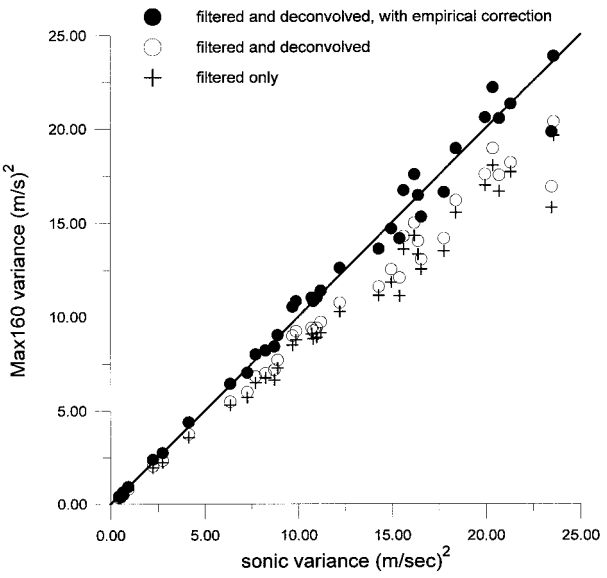

FIG. 8. Sonic variance plotted vs cup variance: filtered only (crosses), filtered and deconvolved (open circles), and filtered and deconvolved with empirical correction (filled circles).

$$S_c(t) = (\tilde{S}(t) - \overline{S}) * 1.08 + \overline{S}, \qquad (15)$$

where the 1.08 is an empirical correction factor determined by trial and error, $\overline{S}$ is the average deconvolved speed over the half-hour interval, $\tilde{S}(t)$ is the deconvolved speed, and $S_c(t)$ is the corrected deconvolved speed. This simple correction improved the variance for all cases; see Table 4 and Fig. 8 in which the corrected variances are plotted as filled-in circles. [Henceforth, we shall present FD wind speeds corrected using Eq. (15).] We do not know if this correction factor would be peculiar to this particular wind regime, or whether it could be applied to all winds measured by the cup at other sites.

TABLE 4. Variances—Tehachapi Pass data.

Case	Sonic variance (m s^{-1})	Max160 σ^2 unfiltered (m s^{-1})^2	Max160 σ^2 filtered (m s^{-1})^2	Max160 σ^2 filtered, deconvolved (m s^{-1})^2	Max160 σ^2 filtered, deconvolved, corrected (m s^{-1})^2
1	0.92	1.4	0.76	0.80	0.94
2	23.6	20.3	19.6	20.3	23.9

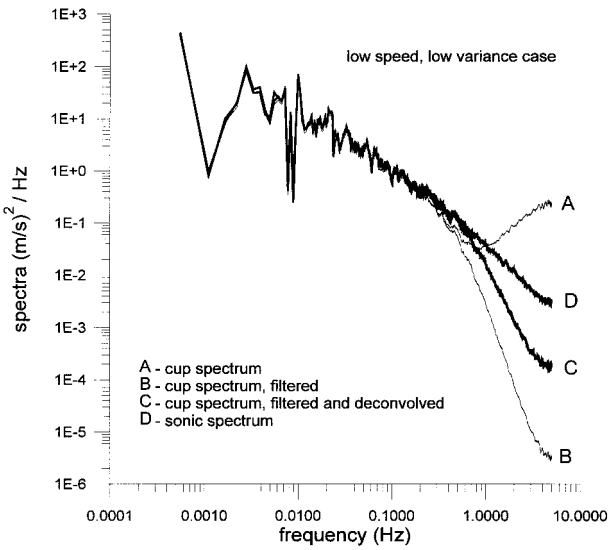

FIG. 9. Spectra of the sonic anemometer (D) and cup anemometer. Case 1: low speed and low variance. Curve A is the cup spectrum before filtering and deconvolution has been applied. Curve B is the cup spectra after filtering, and curve C is after filtering and deconvolution.

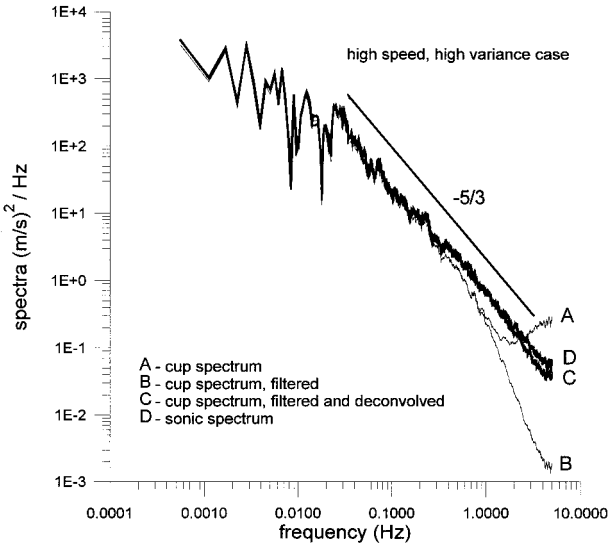

FIG. 10. Spectra of the sonic anemometer (D) and cup anemometer. Case 2: high speed and high variance. Curve A is the cup spectrum before filtering and deconvolution has been applied. Curve B is the cup spectra after filtering, and curve C is after filtering and deconvolution.

Because the correction seemed to work over a range of variances and speeds, we suspect the latter.

The next issue we examine is the equivalency of the sonic and the FD spectra. Figures 9 and 10 show the spectra for cases 1 and 2, respectively. In each figure, four spectra are shown as indicated by the labels A, B, C, and D. These labels refer to the spectrum without filtering (A); with filtering only (B); with filtering, deconvolution, and correction (C); and the sonic spectrum (D). The display of all four spectra clearly shows how the filtering and deconvolution affect the spectra. The filtering reduces any trace of the discretization noise (compare curves A and B), and the deconvolution restores some of the high frequencies that are lost because of the instrument response and filtering (cf. curves B and C). If the FD process is to be of any use whatsoever, then the FD spectrum (C) and the sonic spectrum (D) must be fairly close. In Fig. 9, the cup and sonic spectra are nearly identical up to a frequency of about 1 Hz, at which point the cup spectra falls off. In Fig. 10 the spectra match almost exactly over the entire range of frequencies. (Note that the sonic spectra exhibits the celebrated $-5/3$ law for frequencies above about 0.01 Hz.) Most of the medium- to high-speed cases, those cases most relevant to the wind energy community, exhibit a match this close or even better. The question now becomes, why does the low-speed, low-variance FD spectrum peel away from the sonic spectrum at the higher frequencies?

This difficulty appears to be caused by two factors. First, when the uncorrupted speed has an intrinsic low variance, the signal-to-noise ratio (α, introduced above) becomes small and the filter broadens. This broadening squelches the high-frequency part of the spectrum to such an extent that the deconvolution cannot fully restore the spectrum in this region. That this is the case is certainly evident in Fig. 9. Second, as pointed out by Wyngaard (1981), the response of the instrument for a given speed is characterized by its time constant, defined as simply the distance constant divided by the speed, or D/S. As the speed increases, the cup's time constant becomes smaller, and the cup can track the fluctuations in the true speed with greater fidelity. Thus, for high-speed flows, the need for deconvolution is reduced because the cup's response is faster.

Finally, in Fig. 11 we show a section of the sonic and cup (FD) time series. This figure illustrates some important aspects about the limits of the FD methodology. Perhaps the most important aspect of this plot is the ability of the FD speed to track the sonic speed fairly closely; however, the cup cannot capture the very rapid changes in the speed that are occasionally evident in the time series of the sonic speed. This is particularly evident at time $t = 782$, when a gust exhibits a rapid change in speed over a period of a few seconds. The sonic picks up this change, while the cup does not. There are, however, a few cases in which the cup does track similar bursts.

6. Conclusions

The conclusions from this study may be summarized as follows.

1) An optimal filter to reduce discretization noise from rapidly sampled AC output anemometers is easy to construct and simple to implement. A comparison

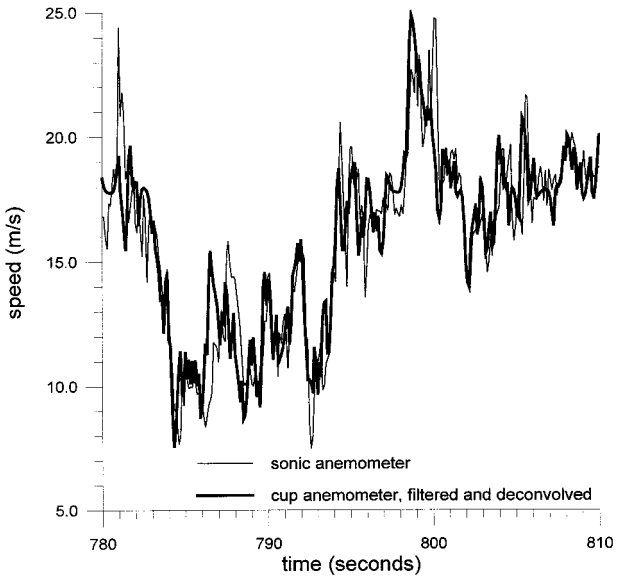

FIG. 11. Section of the time series for the high-speed, high-variance case (case 2). The sonic speed is represented by the thin line and the cup speed (after filtering and deconvolution) is represented by the thick line.

between wind speed time series from a filtered AC output anemometer and a nearby DC output anemometer, not subject to discretization noise, was conducted. Both anemometers were sampled at 5 Hz. The comparison demonstrated that the filter is effective in reducing the discretization noise while retaining the nature of the uncorrupted speed. This is particularly true for flows with a relatively large variance.

2) The anemometer response can be (partially) removed from the filtered time series by a very simple deconvolution procedure. The effectiveness of this procedure was assessed by comparing filtered and deconvolved wind speed time series from an AC output cup anemometer to corresponding time series obtained from a sonic anemometer. Both anemometers were sampled at 10 Hz. The filtered and deconvolved time series exhibited a variance about 10% less than the sonic variance. This lack of correspondence was corrected by a simple empirical correction (although we do not know if this correction would apply in all wind conditions). For the high-speed, high-variance flows relevant to the wind energy industry, the spectra obtained from the filtered and deconvolved time series match the shape of the sonic spectra reasonably well. An examination of the two time series reveals that the cup time series is sometimes not able to capture rapid changes in the wind speed. To capture such quick bursts, a sonic anemometer is necessary.
3) The techniques presented here are most appropriate for wind energy studies in which the high wind speed reduces the time constant of the cup anemometer so that it becomes more responsive.
4) Inexpensive and rugged cup AC output anemometers could be used as replacements for sonic instruments in prolonged field studies if one is aware of the caveats expressed in points 2 and 3 above. For detailed and highly accurate measurements of the turbulent wind field, a sonic anemometer would still be the instrument of choice.
5) The techniques presented here provide the wind energy community with an opportunity to use AC output anemometers to measure some aspects of the turbulent wind. The primary advantage of this technique is cost: AC anemometers are often much less expensive than comparable DC output anemometers and certainly less expensive than sonic anemometers. Other important advantages include flexibility and familiarity. The industry has considerable experience using AC output anemometers, and this familiarity has fostered confidence in the performance of these anemometers. In the past these anemometers were thought to be only useful for resource assessment or turbine control; now these anemometers can be used for some turbulence measurements as well.

Acknowledgments. This work was supported by the U.S. Department of Energy under contract DE-AC06-76RLO 1830. The Pacific Northwest National Laboratory is operated for the U.S. Department of Energy by the Battelle Memorial Institute. The authors appreciate the efforts of staff members at the National Renewable Energy Laboratory, who provided us with a sonic anemometer and helped install this instrument prior to the sonic/cup comparison field campaign.

APPENDIX

An Estimate of Cup Overspeeding

To further examine the issue of cup anemometer overspeeding we follow the work of Kristensen (1992). Cup anemometer overspeeding is composed of four biases. The first three are the so-called u, v, and w biases. The u bias may be attributed to fluctuations of the wind along the mean direction, while the v and w biases are caused by velocity fluctuations perpendicular to the mean direction, either in the horizontal direction (v bias) or vertical direction (w bias). Additionally, there is a stress bias proportional to total horizontal stress. As pointed out by Kristensen (1992), the stress bias and the u bias are most effected by the small-scale fluctuations of the wind. Thus, if the u bias is small, the stress bias will likely be small also. The v bias is only nonzero if the measured speed is interpreted as the mean speed along the mean direction (as opposed to the total horizontal speed; see MacCready 1966). With the awareness that our measurements are of the total horizontal speed, we may take the v bias to be zero. The w bias

is proportional to the square of the vertical turbulence intensity.

We can estimate the u bias (δ_u) using Eq. (81) in Kristensen (1992):

$$\delta_u = \frac{a_4}{U^2} \int_{-\infty}^{\infty} \frac{\omega^2 \tau_o^2}{(1 + \omega^2 \tau_o^2)} S_u(\omega)\, d\omega, \qquad \text{(A1)}$$

where constant a_4 is a positive constant less than one (the u bias is always positive), U is the magnitude of the speed in the mean direction, τ_o is the anemometer time constant (equal to the distance constant divided by the wind speed), and $S_u(\omega)$ is the power spectrum of U as a function of the frequency ω. For the estimation of δ_u we assume that τ_o is constant (when in fact it obviously varies as U changes) and that it is equal to the distance constant divided by the mean speed over the time period under consideration.

For case 2 listed in Table 3, we set τ_o equal to 0.19 s [(3 m)/(16 m s^{-1})], we set a_4 equal to one (its upper limit), and we use the sonic spectrum for $S_u(\omega)$. Using Eq. (A1), we find that an upper limit to the u bias is only $+0.4\%$. We assume that the stress bias is of this magnitude or smaller. Kristensen (1992) estimated the stress bias and found that it was very much smaller than the u bias, so this assumption seems justified. The fact that the u bias is small makes sense because the time constant of the instrument is small when the wind speed is high and the anemometer can follow all but the most small-scale fluctuations in speed. This assertion can be made more quantitative by examining the transfer function in Eq. (A1), $(\omega\tau_o)^2/[1 + (\omega\tau_o)^2]$. This function assumes half its maximum value when $\omega\tau_o$ is equal to one, and we can define a frequency, f_o, [$1/(2\pi\tau_o) \approx 0.8$ Hz] above which the eddies contribute to the u bias. A glance at the sonic spectrum in Fig. 10 suggests that these ''contributing'' eddies contain only a small part of the energy of the entire turbulent spectrum; hence, the u bias is small. The small magnitude of the u and stress biases can also be confirmed using the simplified formula of Busch and Kristensen (1976).

It remains to estimate the w bias (δ_w). As shown by Kristensen (1992), this quantity is approximately equal to

$$\delta_w \approx \frac{\langle w^2 \rangle}{U^2}, \qquad \text{(A2)}$$

where a_5 is a constant related to the angular response of the anemometer and $\langle w^2 \rangle$ is the variance of the vertical velocity. (If the anemometer has a perfect cosine response, a_5 is equal to zero.) Using vertical velocity data from the sonic [with $\langle w^2 \rangle$ equal to 7 (m s^{-1})^2—this is a turbulent site!], we estimate that the contribution to overspeeding by the w bias to be about $\pm 2.7\%$. This estimate assumes that a_5 is equal to ± 1, a magnitude that is probably too large [e.g., Kristensen (1992) reports a value for a_5 equal to $+0.67$]. We cannot further refine this estimate without information about the angular response of the anemometer. It is likely that the magnitude of the overspeeding due to vertical velocity fluctuations is less than 2.7%.

Keeping in mind that the estimate of the w bias may be too large, an estimate of the overspeeding due to all causes is $+0.4\% \pm 2.7\%$. If we take the w bias to be positive and half the value of 2.7% (a reasonable assumption), we get an overspeeding error of 1.8%. This estimate is the same as the actual discrepancy between the cup and the sonic anemometers based on measured mean values. Although the close correspondence between these two values is probably coincidental, the results presented here suggest that for high-speed flows the overspeeding is relatively small, even under the very turbulent conditions portrayed by case 2 in Table 3.

REFERENCES

Busch, N. E., and L. Kristensen, 1976: Cup anemometer overspeeding. *J. Appl. Meteor.*, **15,** 1328–1332.

Collins, A., and R. Hunter, 1992: Recovery of cup anemometer incident wind speed using simple on-line algorithms. *Proc. 14th British Wind Energy Conf.*, Nottingham, United Kingdom, British Wind Energy Association, 283–290.

Connell, J. R., 1981: The spectrum of wind speed fluctuations seen by a rotating blade of a wind energy conversion system: Observations and theory. Pacific Northwest National Laboratory, PNL-4083, 66 pp.

George, R. L., and J. R. Connell, 1984: Rotationally sampled wind characteristics and correlations with MOD-OA wind turbine response. Pacific Northwest National Laboratory, PNL-5238, 76 pp.

Kristensen, L., 1992: The cup anemometer and other exciting instruments. Ph.D. dissertation, Riso National Laboratory, 83 pp. [Available from Riso Library, Riso National Laboratory, P.O. Box 49, DK-4000, Roskilde, Denmark.]

——, and D. H. Lenschow, 1988: The effect of nonlinear dynamic forcing response on measured means. *J. Atmos. Oceanic Technol.*, **5,** 34–43.

MacCready, P. B., Jr., 1966: Mean speed measurements in turbulence. *J. Appl. Meteor.*, **5,** 219–225.

Panofsky, H. A., and J. A. Dutton, 1984: *Atmospheric Turbulence.* John Wiley and Sons, 397 pp.

Press, W. H., S. A. Teukolsky, W. T. Vetterling, and B. P. Flannery, 1992: *Numerical Recipes in FORTRAN: The Art of Scientific Computing.* 2d ed. Cambridge University Press, 963 pp.

Veers, P. S., 1988: Three-dimensional wind simulation. Sandia National Laboratories, SAND88-0152, 36 pp.

Wendell, L. L., 1998: Turbulence characterization for wind energy development. National Renewable Energy Laboratory, NREL/SR-500-21980, 146 pp. [Available from National Renewable Energy Laboratory, 1617 Cole Blvd., Golden, CO 80401.]

Wyngaard, J. C., 1981: Cup, propeller, vane, and sonic anemometers in turbulence research. *Annual Review of Fluid Mechanics,* M. Van Dyke, J. V. Wehausen, and J. L. Lumley, Eds., Annual Reviews, 399–423.